BEATS

Workpackage 3

The X-ray Source

Report on super-bend vs. 3-pole wiggler, lattice comparison

D 3.1

July 2020

Funded by the EU's H2020 framework programme under grant agreement n°822535

PROJECT DETAILS

PROJECT ACRONYM
BEATS

PROJECT TITLE
BEAmline for Tomography at SESAME

GRANT AGREEMENT NO:
822535

THEME

START DATE
2019

DELIVERABLE DETAILS

WORK PACKAGE: 03

EXPECTED DATE: 31/07/2020

WORK PACKAGE TITLE: THE X-RAY SOURCE

DELIVERABLE TITLE:REPORT ON SUPERBEND VS. 3-POLE-WIGGLER, LATTICE COMPARISON

WORK PACKAGE LEADER: INFN

DELIVERABLE DESCRIPTION: REPORT

DELIVERABLE ID: D3.1

PERSON RESPONSIBLE FOR THE DELIVERABLE: A. GHIGO

NATURE

☒ R - Report ☐ P - Prototype ☐ D - Demonstrator ☐ O - Other

DISSEMINATION LEVEL

☒ P - Public
☐ PP - Restricted to other programme participants & EC:
☐ RE - Restricted to a group
☐ CO - Confidential, only for members of the consortium

REPORT DETAILS

VERSION: 2

DATE: 31/07/2020

NUMBER OF PAGES: 28

DELIVERABLE REPORT AUTHOR(S): A. GHIGO, J. CAMPMANY ET AL.

FOR MORE INFO PLEASE CONTACT: ANDREA.GHIGO@LNF.INFN.IT

STATUS

☐ Template ☐ Draft
☒ Final ☒ Released to the EC

Contents

INTRODUCTION

The tasks of the BEATS project's Work Package 3 are as follows:

- to identify the optimal x-ray source by choosing from established concepts based either on a super-bend, a multipole wiggler, or a 3-pole wiggler structure (super-bend and 3-pole wiggler operating at a field of 3T) and
- to perform a design study for the chosen source type

In this report, a comparison between these options is carried out, based on the results of investigations presented at the BEATS kick-off meeting held in March 2019 [1, 2] and on the work done within Work Package 3 in the following months.

The major requirements for the BEATS x-ray source are:

- The critical photon energy of the emitted x-ray spectrum should be considerably higher than that of the existing storage ring dipoles,
- Flux and brightness of the photon beam need to be maximized.
- To achieve the latter, corrective measures on the machine optics need to be foreseen to reduce the emittance of the electron beam.

The following constraints need to be taken into account:

- The electrons are injected into the storage ring at low energy (800MeV)
- Following injection, the beam is ramped up in the storage ring to a final energy of 2.5 GeV.
- Reduce as much as possible the necessary modification to the storage ring optics.
- The project overall time planning leaves only a relatively short time to make a choice and to prepare the source design (4+2 months). This is due to the fact that other activities (design of the front end and the beamline optics) depend on the characteristics of the x-ray source.

THE SUPER-BEND OPTION

In this section we describe in detail the option to replace one of the ring dipole magnets with a 3 T super-bend in.

A comparison between the key parameters of a standard SESAME dipole [3] and the envisaged super-bend is given in Table 1.

	Ring dipole	Super-bend
Max B (T)	1.455	3.0
Length (m)	2.25	1.0916
Gradient (T/m)	-2.79	0.0

Table 1: Key parameters of standard SESAME ring dipoles and the super-bend

Standard SESAME storage ring bending magnets are combined-function magnets with magnetic field B=1.455 T, gradient G = -2.79 T/m, curvature radius ρ = 5.73 m, and magnetic length L = 2.25 m. The critical photon energy of the x-ray spectrum emitted by these dipoles is 6 keV. The basic concept of the super-bend option is to replace one standard magnet by a 3 T dipole which would shift the critical photon energy to 12.5 keV.

The goal of obtaining a magnetic field of 3 T in a normal conducting dipole magnet necessitates a pure dipole (i.e. without gradient) in order to have more freedom to reduce the gap as much as possible. The 3 T parallel face super-bend would have a magnetic length L = 1.09 m and a bending radius ρ = 2.8 m. The existing defocusing quadrupoles are not strong enough to compensate the loss of vertical focusing with respect to the standard bend.

Therefore, two 0.1 m long defocusing quadrupoles on both sides of the super-bend would need to be replaced by two stronger 0.2 m long quadrupoles (called here QDSB). Figure 1 shows the SESAME storage ring lattice with one standard dipole replaced by a super-bend: standard focusing quadrupoles are shown in red, standard defocusing ones in blue and the two new defocusing QDSB in magenta.

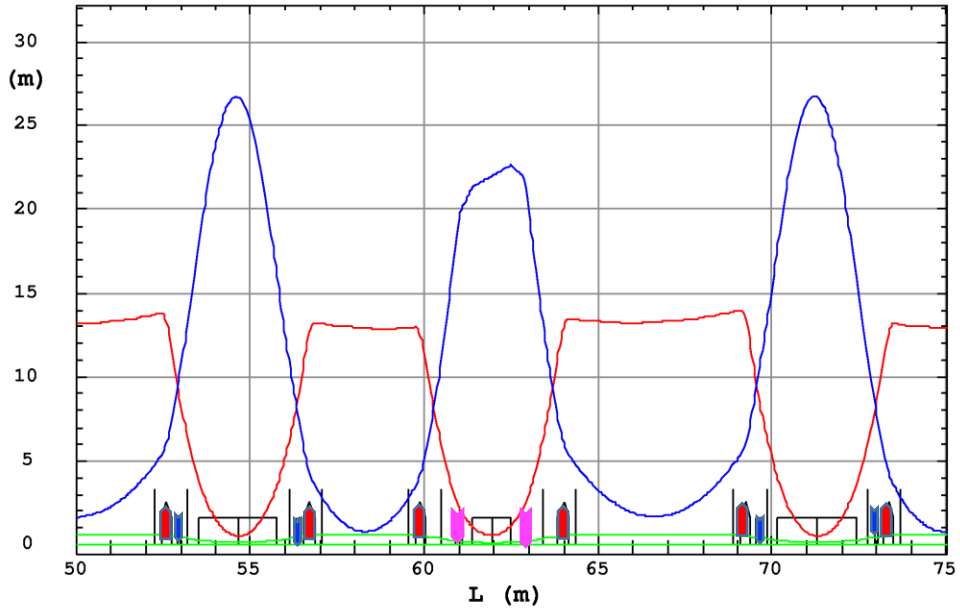

Figure 1: The SESAME storage ring optics with a super-bend inserted in the centre of the cell. Red line: horizontal betatron function β_x,, blue line: vertical betatron function β_y , and green line: dispersion η_x. New defocusing 0.2 m long quadrupole magnets are inserted on both sides of the super-bend replacing the original ones of 0.1 m length.

The resulting optical disturbance and its compensation

Inserting the super-bend in the lattice highly distorts the linear optics. The original optical compensation scheme is a global one, inserting the super-bend requires a modification of the strength of 10 quadrupole pairs as follows:

- The four quadrupoles in the super-bend cell (cell 8: two existing QF together with the two new QDSB magnets) and
- the four existing quadrupoles (two QF and two QD) in each of the 4 cells adjacent to the super-bend cell (cells 6, 7, 9,10),
- and the two original families in the rest of the ring [3].

This way it is possible to compensate the vertical beta-beating down to $\Delta\beta_y/\beta_y$ = 1.9% and the horizontal beta-beating down to $\Delta\beta_x/\beta_x$ = 3%. The dispersion beating is reduced to $\Delta\eta_x/\eta_x$ = 0.75% (i.e. $\Delta\eta_x \approx$ 4mm) everywhere except in the straight sections around the super-bend where dispersion is reduced by 1.4 cm. Figure 2 shows the betatron functions (top) and dispersion (bottom) after optical compensation.

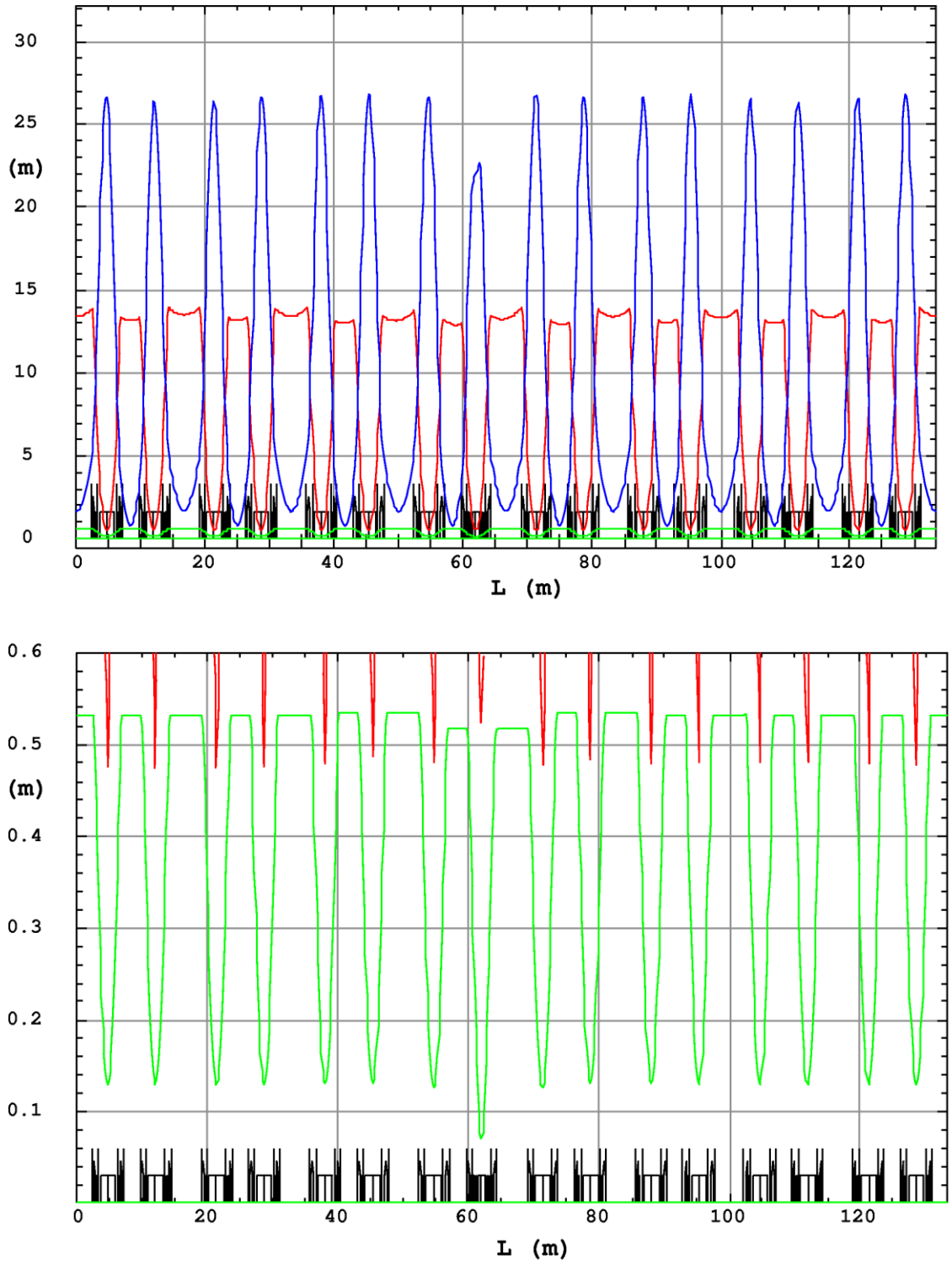

Figure 2: The distortion compensated optics for betatron functions (top) and dispersion (bottom).

Table 2 lists the resulting variation of the gradients of the storage ring quadrupoles with and without the super-bend. The quadrupole called QDSB is the new inserted defocusing one in the super-bend cell (cell 8), the other quadrupole families are identified by the number of the cell: QF6 (focusing, cell 6) and QD6 (defocusing, cell 6).

Quadrupole family	Original gradient (T/m)	Gradient (T/m) with super-bend
QF6 (L = 0.3 m)	16.6	16.58
QD6 (L = 0.1 m)	-8.3	-8.26
QDSB (L = 0.2 m)	-	-17.1
QF8	-	15.74
QF7	-	16.73
QD7	-	-8.54
QF9	-	16.53
QD9	-	-8.21
QF10	-	16.6
QD10	-	-8.33

Table 2: modification of the quadrupole strength of the SESAME lattice needed to compensate for the distortion by a super-bend.

The resulting reduction of the dynamic aperture caused by the introduction of the super-bend is minimized by the compensation of dispersion beating. Figure 3 shows the resulting ideal (i.e. error free) dynamic aperture of a lattice with the super-bend (for a particle tracked for 1000 turns) compared to the original one. However, there is still the possibility to further increase the dynamic aperture by combining the sextupoles around the super-bend in different families and fine-tune them with respect to the other sextupoles in the ring.

The reduction in the dynamic aperture is still small taking into account the machine physical aperture which is defined horizontally by the injection septum and vertically by the vacuum chamber height in bending magnets.

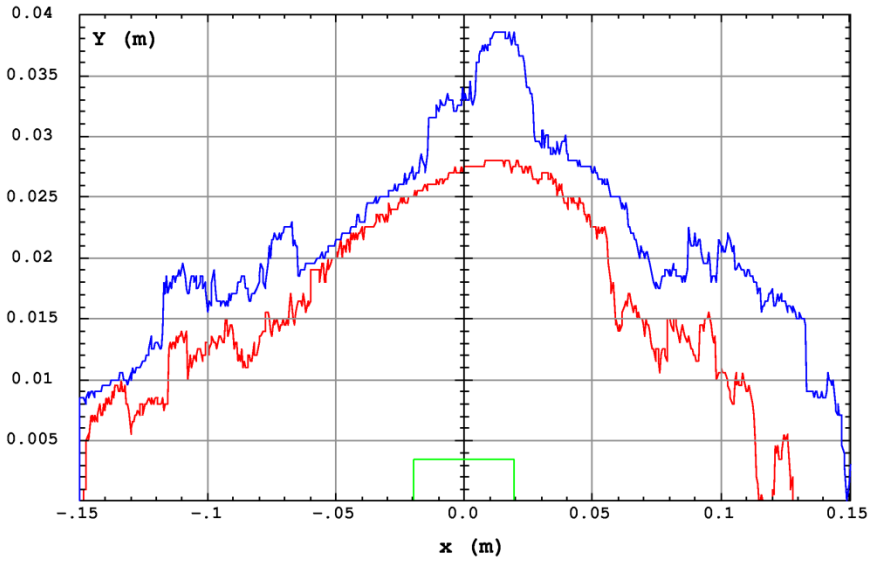

Figure 3: The ideal dynamic aperture with super-bend (red) compared to the original one (blue) for particle tracked for 1000 turns. The physical aperture is shown in green.

Impact of the super-bend on the main machine parameters and photon brilliance

The main parameters of the machine with and without the super-bend are listed in Table 3.

	Original lattice	Super/bend
Emittance (nm·rad)	26.1	27.2
Energy loss/turn (keV)	603.6	643.6
Energy spread (%)	0.108	0.112
Damping time x,y,s (ms)	2.2, 3.7, 2.7	2.2, 3.4, 2.4

Table 3: Lattice main parameters without/with Super-bend

The values of beam size and divergence at the centre of the super-bend are:

σ_x = 143.3μm, σ_x' = 228.2 μrad, σ_y = 77.4 μm and σ_y' = 4.1 μrad.

The Twiss parameters at the center of the super-bend are β_x = 0.523 m, α_x= -0.037, η_x = 0.071 m, η'_x = -5.5e-5, β_y = 22 m, α_y = -0.6, and the resulting values of the electron beam size and divergence at that point are σ_x = 143.3μm, σ_x' = 228.2 μrad, σ_y = 77.4 μm and σ_y' = 4.1 μrad. This results in a peak photon brilliance of 3.5 x10^{14} (ph/s.mm^2.mrad^2.0.1%BW) for 200 mA electron beam current as shown in Figure 4.

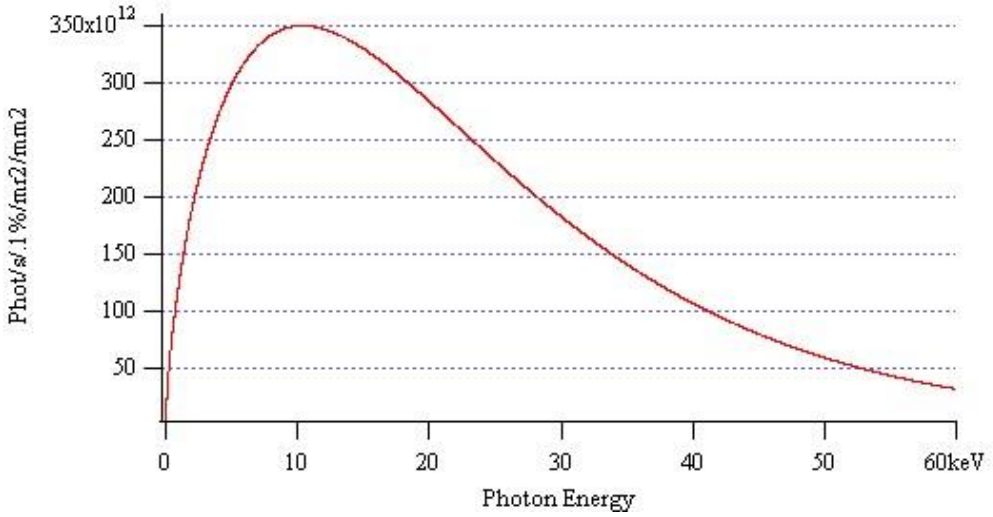

Figure 4: The photon brilliance as a function of energy for 200mA electron current from the 3 T super-bend in the SESAME storage ring.

This can be compared to the brilliance from the original SESAME bending magnet as shown in Figure 5, where the photon source is located at 6.5 deg from the dipole exit. The corresponding Twiss parameters are β_x = 0.955 m, α_x= -1.078, η_x = 0.153 m, η'_x = 0.103, β_y = 24.1 m, α_y = 4.513,

and the resulting electron beam sizes and divergences there are σ_x = 228.4 μm σ_x' = 265.9 μrad, σ_y = 78.7 μm and σ_y' = 15.1 μrad.

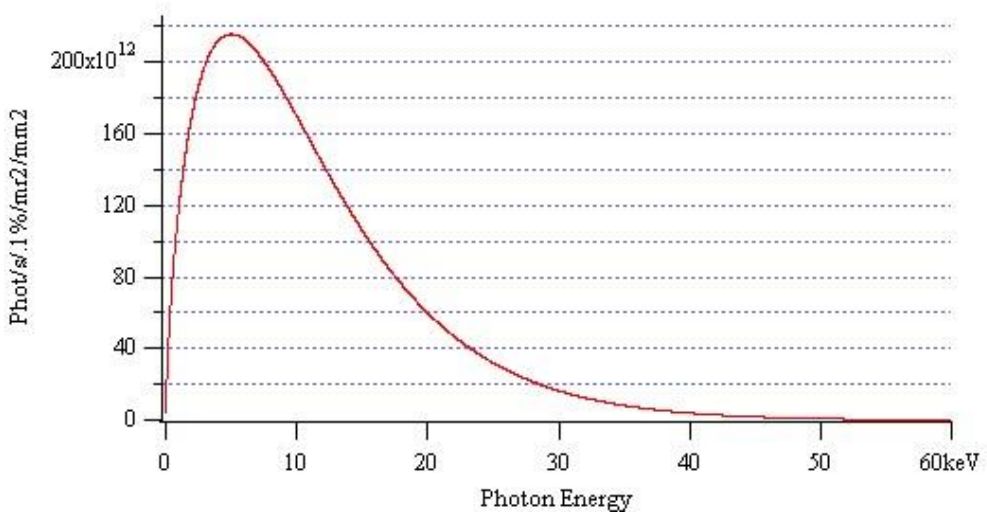

Figure 5: The photon brilliance as a function of energy for 200mA electron current emitted by a standard SESAME bending magnet.

The additional power loss of 4 kW/100mA due to the super-bend has to be taken into account in the design of the crotch absorber. Furthermore, the super-bend leads to an increase of the required RF power by 6.7 %.

In summary: The installation of a super-bend has tolerable effect on the dynamical aperture, when considering an ideal case without errors, and its perturbation of the lattice can be limited. To have a better estimate of the dynamic aperture a detailed design of the magnet would be needed, in order to take into account the high order terms of the magnetic field expansion.

However, even if the effect on the dynamic aperture is tolerable, the insertion of a super-bend has a considerable impact on the accelerator:

- Two new quadrupoles and a new vacuum chamber in the super-bend cell are needed.
- The existing girder either needs considerable mechanical modifications in order to accommodate the super-bend and two new quadrupoles or, alternatively, a new girder has to be designed and built, requiring a long shutdown of SESAME.

THE MULTIPOLE WIGGLER OPTION

The aforementioned disadvantages of a super-bend can be avoided by using a 3 T multipole (50 poles) wiggler as an alternative photon source for the tomography beamline, which could be accommodated in one of the long straight sections. The assumed parameters of the investigated wiggler are: peak field B = 3T, period λ_w = 50 mm, and length L = 2.5 m. The corresponding deflection coefficient is K = 14.

The high value for the dispersion of 0.53 m in SESAME's straight sections could increase the impact of the wiggler on the storage ring's energy spread and emittance, in particular if one takes into account the other wigglers that will be installed (for instance, the wiggler of the Material Science Beamline featuring B = 1.38 T, λ_w = 60.5 mm, and length L = 2 m). Hence, the influence of the value of the dispersion in the straight sections has to be investigated.

Comparison of optics with different values of the dispersion in the long straight sections

The SESAME storage ring is of 8-fold symmetry with 16 straight sections, 8 long sections of 4.4 m length and 8 short ones of 2.4 m length. The storage ring lattice is simple with only two families of quadrupoles as shown in ref. [3]

Due to the 8-fold symmetry and the non-flexible structure of the storage ring lattice, the most direct and easy way to control dispersion is to modify it equally in 8 straight sections, which can be done with tolerable changes in quadrupole strength. Unfortunately, reducing the dispersion in the long straight sections increases the dispersion in the short straight sections. Table 4 shows the case of zero dispersion in the 8 long straight sections which result in high dispersion in short sections.

zero-disp. Sections	Emitt. (nm.rad)	η_x (m) in short sections	Quad families used	Max $\Delta k/k$
8 long sections	49	1.02	6	14%QD, -0.2%QF

Table 4: Machine parameters for the case of zero dispersion in the 8 long straight sections

Table 5 lists the relevant parameters for different values of the dispersion in the long 8 sections without and with wigglers as calculated using the BETA code. It also lists the value of the beam size (1 rms) in long and short straight sections. The Material Science Beamline wiggler is taken into account, too. The variation of the Twiss parameters when introducing wigglers are not considered since it is assumed that they can well be recovered by the optical compensation method.

Case	Emittance	η_x (long sec)	η_x (short sec)	Energy spread	σ_x (long) µm	σ_x (short) µm
Zero dispersion in long sections						
No wiggler	49.4 nm.rad	0.01 m	1.01 m	1.06 x10^{-3}	864	1320
3T Wiggler	45.2 nm.rad	0.01 m	1.01 m	1.08 x10^{-3}	826	1319
3T+1.38T wigg	44.5 nm.rad	0.01 m	1.01 m	1.08 x10^{-3}	820	1311
10 cm dispersion in long sections						
No wiggler	41.9 nm.rad	0.1 m	0.925 m	1.07 x10^{-3}	797.6	1223
3T+1.38T wigg	37.9 nm.rad	0.1 m	0.925 m	1.084 x10^{-3}	759	1212
20 cm dispersion in long sections						
No wiggler	35.9 nm.rad	0.2 m	0.842 m	1.076 x10^{-3}	762	1126
3T+1.38T wigg	32.9 nm.rad	0.206m	0.837	1.089 x10^{-3}	734	1114
30 cm dispersion in long sections						
No wiggler	31.5 nm.rad	0.3 m	0.758 m	1.08 x10^{-3}	760	1034
3T+1.38T wigg	30.0 nm.rad	0.3 m	0.759 m	1.092 x10^{-3}	747	1033
40 cm dispersion in long sections						
No wiggler	28.7 nm.rad	0.4 m	0.676 m	1.084 x10^{-3}	790	950
3T+1.38T wigg	28.6 nm.rad	0.399 m	0.677 m	1.095 x10^{-3}	790	956
Original optics (disp = 0.53 m)						
No wiggler	26 nm.rad	0.53 m	0.53 m	1.086 x10^{-3}	827	822
3T+1.38T wigg	28.8 nm.rad	0.53 m	0.53 m	1.096 x10^{-3}	853	847

Table 5: Relevant machine parameters for different wiggler combinations and different values of the dispersion

Table 6 lists the Twiss parameters of the bare lattice (i.e. without wiggler) in the long straight sections. The value of the vertical beam size is calculated assuming 1% coupling.

β_x (m)	α_x	β_y (m)	α_y	η_x (m)	η'_x	σ_x (μm)	σ_y (μm)
Zero dispersion in long sections							
15.1	0	1.6	0	0.01	0	864	28.1
10 cm dispersion in long sections							
14.9	0	1.6	0	0.1	0	797.6	25.9
20 cm dispersion in long sections							
14.9	0	1.61	0	0.2	0	762	24.1
30 cm dispersion in long sections							
15	0	1.62	0	0.3	0	760	22.6
40 cm dispersion in long sections							
15.2	0	1.62	0	0.4	0	790	21.6
Original optics (dispersion = 0.53 m)							
13.5	0	1.65	0	0.53	0	827	20.7

Table 6: Twiss parameters for the bare lattice in the long straight sections for different values of the dispersion

Using the results listed in Tables 5 and 6, the photon beam's brilliance at critical energy emitted by the wiggler was calculated for values of the dispersion (Table 7). Values for the electron beam size and divergence at the source point are listed as well. For these calculations the Twiss parameters of the bare lattice (which are assumed to be recovered after optical compensation) were used, whereas for the energy spread and emittance values affected by the presence of wigglers are taken into account.

Optics	Brilliance from 3T wiggler	σ_x (μm)	σ_x' (μrad)	σ_y (μm)	σ_y' (μrad)
Zero disp	1.767 x10^{16}	819.8	54.3	26.7	16.7
10cm disp	2.069 x10^{16}	759.2	50.4	24.6	15.4
20cm disp	2.294 x10^{16}	733.2	47	23	14.3
30cm disp	2.353 x10^{16}	746.5	44.7	22	13.6
40cm disp	2.273 x10^{16}	791.6	43.4	21.5	13.3
original	2.085 x10^{16}	852.2	46.2	21.8	13.2

Table 7: Brilliance, electron beam size and divergence for different values of the long straight section dispersion

These results show that the case of 30 cm dispersion in the long straight sections is the optimal choice to be adopted for the SESAME operational optics with the mentioned wigglers.

The photon spectrum emitted by the 3 T wiggler (located in the 30cm dispersion section) is shown in Figure 6.

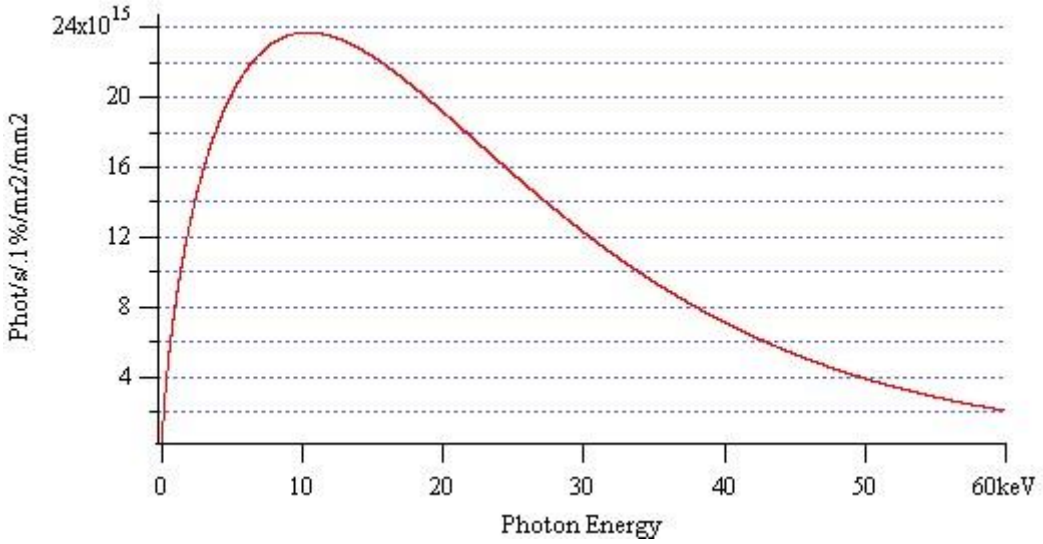

Figure 6: The brilliance of the photon beam as function of the energy for 200mA current from the 3 T multipole wiggler.

The photon brilliance from the 3 T multipole wiggler is 68 times higher than that from the 3 T super-bend.

Compensation of the multipole wiggler's optical disturbance

The modification of the emittance and the energy spread by the multipole wiggler as listed in Table 5 is not the only distortion of the optics. One has to take into account as well the effect created by the two other wigglers currently installed at SESAME (3T and 1.38T), in a lattice with 30 cm dispersion in the long straight sections. These lead to a vertical tune shift of $\Delta Q_y = 0.026$ and to an optical distortion shown in Figure. 7.

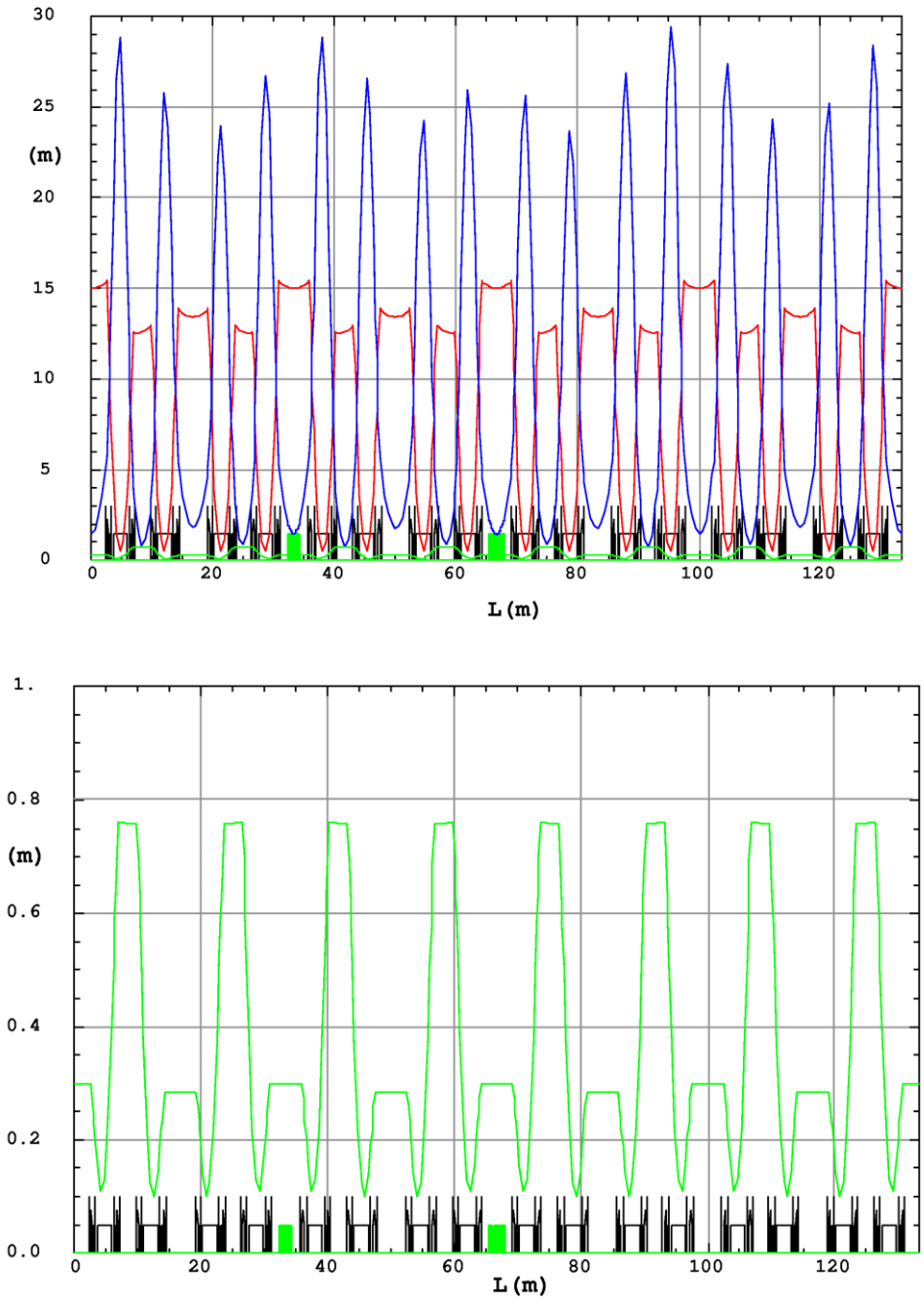

Figure 7: The distortion of betatron functions β_x (red) and β_y (blue) (top), and the dispersion function (bottom) due to the effects caused by the wigglers of the BEATS and the Materials Science beamlines.

The wigglers' optical distortion can easily be compensated utilizing the global correction scheme where two new quadrupole families are introduced around each wiggler and used together with the existing 6 families (10 families in total) to correct tunes and Twiss parameters in the ring. The maximum increase in quadrupole strength needed for the optical correction is 2.5% in QF and 3% in QD which is within the range of the existing power supplies. The machine optics after compensation is shown in Figure 8.

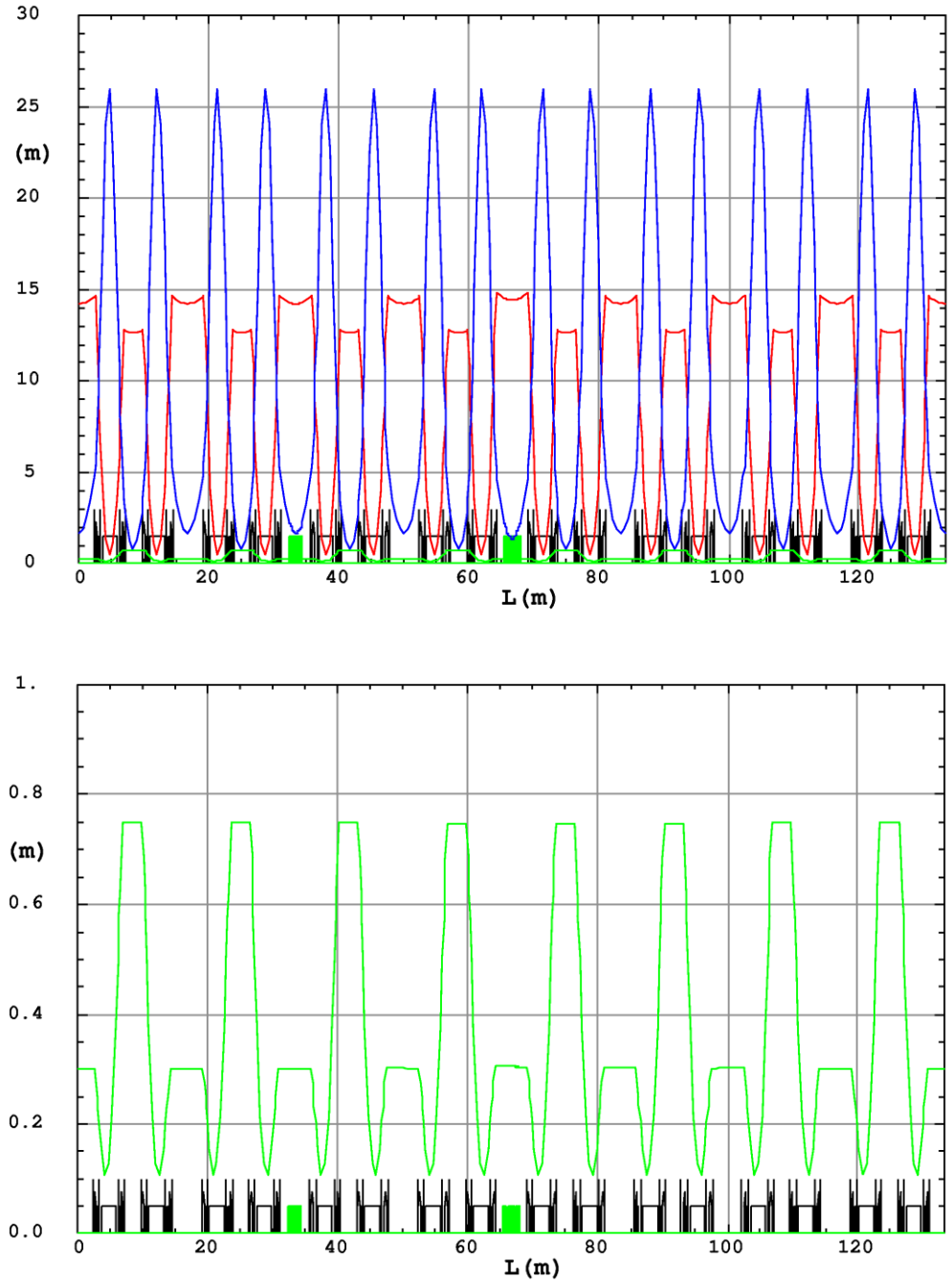

Figure 8: The machine optics after compensation of the disturbance of the BEATS' and the existing beamlines' wigglers.

Table 8 shows a comparison between the Twiss parameters and the beam size for the cases without wigglers and with wigglers after compensating their optical disturbance.

	β_x (m)	α_x	β_y (m)	α_y	η_x (m)	η'_x	σ_x (μm)	σ_y (μm)
Without wigglers	15	0	1.62	0	0.3	0	760	22.6
With wigglers	14.2	0	1.68	0	0.3	0	727	22.3

Table 8: Comparison of Twiss parameters and beam size for a lattice with and without wigglers

Nonlinear impact of the multipole wiggler

The wigglers' impact on the ideal dynamic aperture is shown in Figure 9 for a particle tracked over 1000 turns and chromaticity corrected to zero in both planes using only two families of sextupoles.

Although the dynamic aperture is considerably reduced, it is still well beyond the physical aperture represented by the green box.

In summary: The installation of a multipole wiggler has tolerable effect on the dynamical aperture, when considering an ideal case without errors, and its perturbance of the lattice can be limited. To have a better estimate of the dynamic aperture a detailed design of the wiggler would be needed, in order to investigate as well the high order terms of the magnetic field expansion. At present no wiggler design is available and it is expected that such a design can be achieved only using superconducting technology, which the SESAME infrastructure currently does not support.

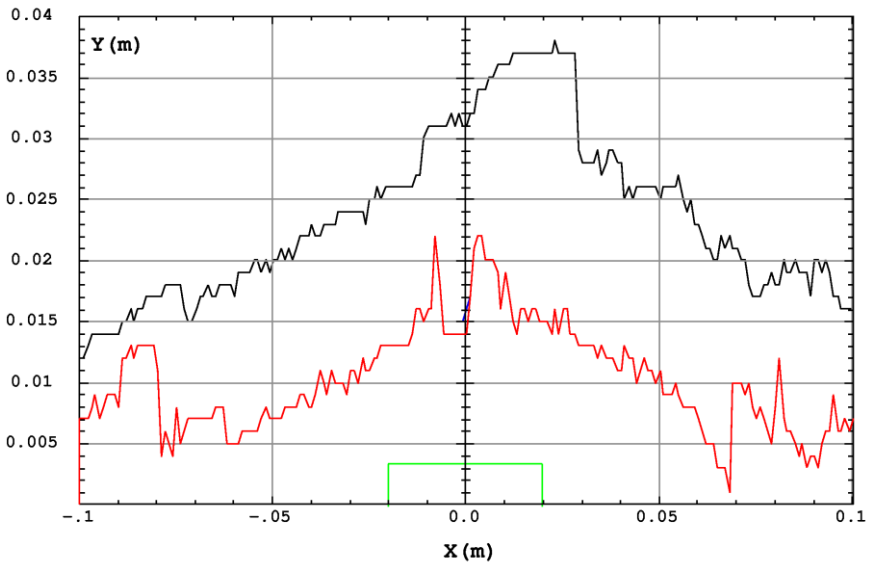

Figure 9: The error-free dynamic aperture without (black) and with (red) wigglers using chromaticity corrected to zero in both planes, and calculated for particle tracked 1000 turns. Green: Physical aperture.

THE 3 T WAVELENGTH SHIFTER (3-POLE WIGGLER) OPTION

A third option is to use a 3 T wavelength shifter composed of two low field side dipoles at the entrance and the exit of the device and a strong dipole in the centre of the device, allowing for a substantially increased critical energy of the emitted photon spectrum.

The design of such a device was already available [5] at the time of the BEATS kick-off meeting. It allows to achieve a peak field of 3 T by using permanent magnets. The installation of this wiggler would have a minimal impact on the SESAME technical systems since it is small and does not require any power supply.

As a first estimation of the photon spectrum emitted by such a device, the magnetic field was modelled by assuming

- a central dipole of B = 3 T, L = 0.1 m
- two side dipoles of B = 0.2 T, L = 0.75 m acting as lateral collectors

The resulting model flux distribution is shown in Figure 10.

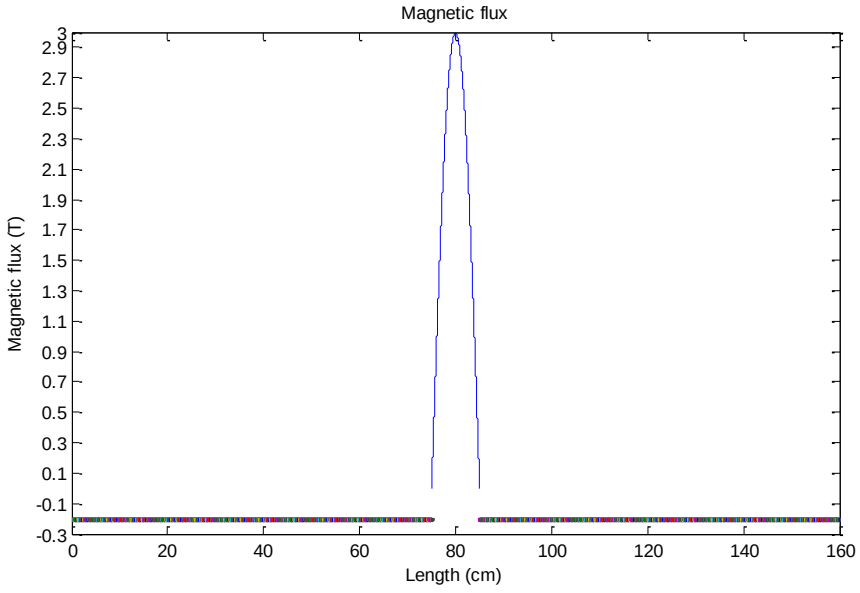

Figure 10: Flux distribution of the first model of the 3T wavelength shifter.

This option has the advantage of using a single photon source. The magnetic flux in the side dipoles (B= 0.2 T) produces photons with critical energy of only 0.83 keV. This leads to sufficient spectral

separation from radiation of the central dipole whose critical energy is 12.5 keV (assuming the photon spectral range to be 5 – 50 keV), see Figure 11.

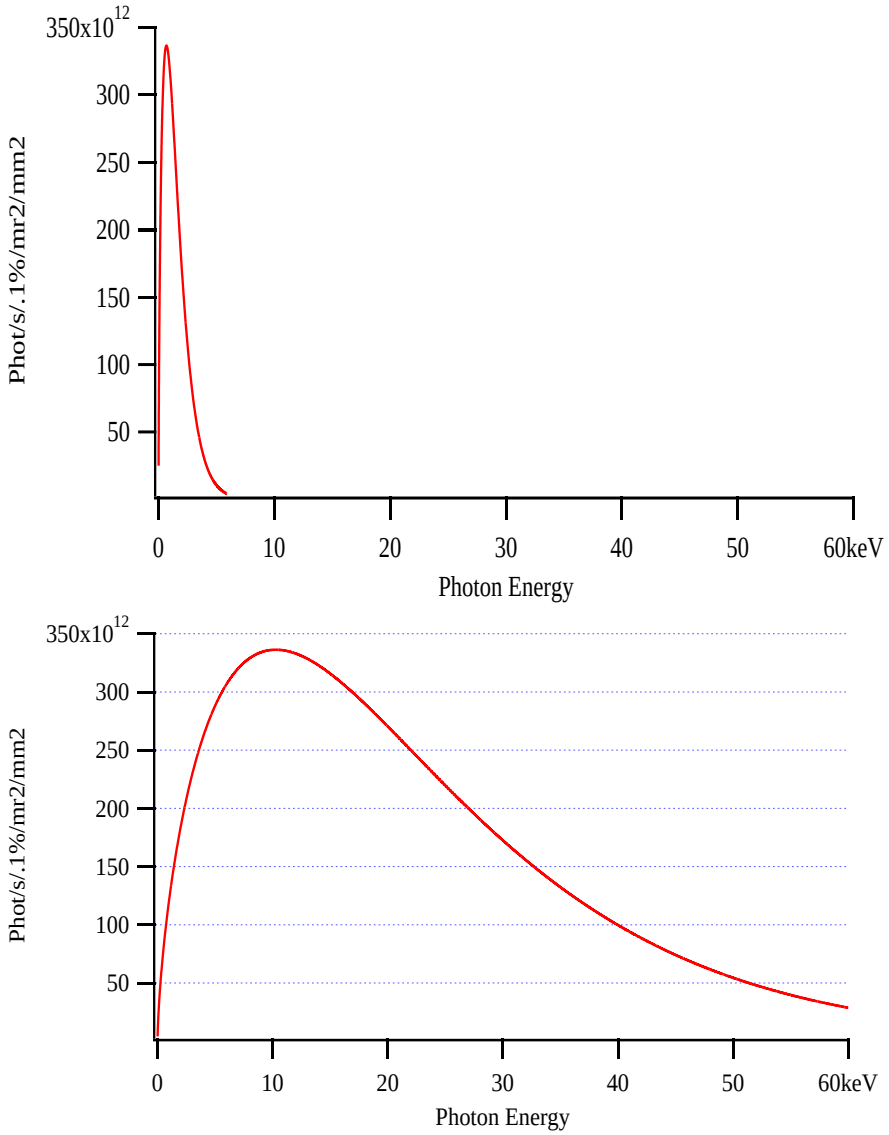

Figure 11: Spectral separation between side and central dipoles of the wavelength shifter. Top: emission from the side dipoles, bottom: emission from the central dipole

Design of the 3-pole wavelength shifter (3PW-1)

A refined design of a 3-pole wiggler, out of vacuum, with 3 T peak field and 11 mm gap was proposed during the first months of the activity of work package 3 [5]. The magnetic model of this wiggler, called 3PW-1, is shown in Figure 12. Figure 13 depicts the vertical magnetic field on axis, Figure. 14 the field integral along the transversal axis.

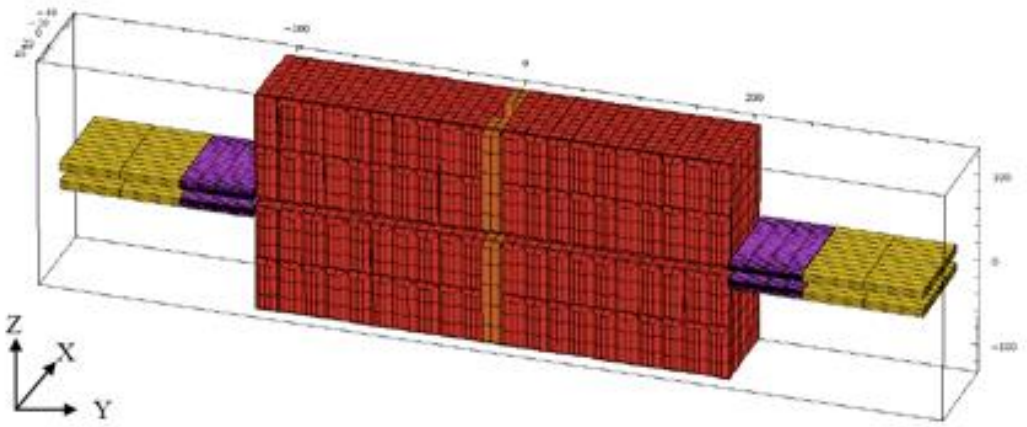

Figure 12: Magnetic model of 3PW-1, generated by RADIA. Red, yellow and orange parts are NdFeB magnets, pink parts are iron poles. The overall length is 0.755 m.

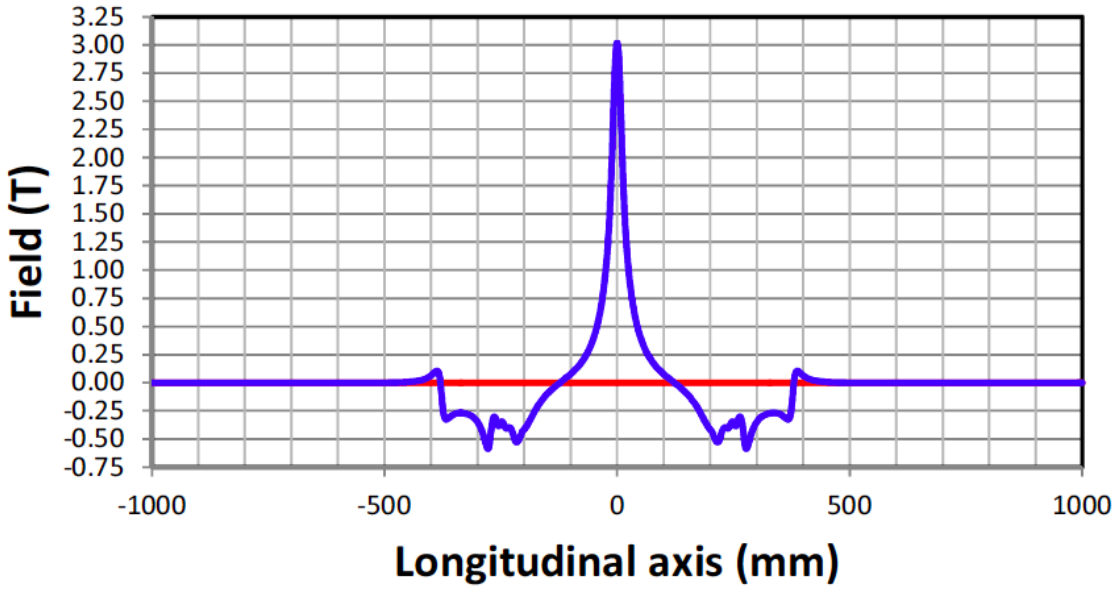

Figure 13: Magnetic field of the 3T wavelength shifter along the trajectory of the electron beam.

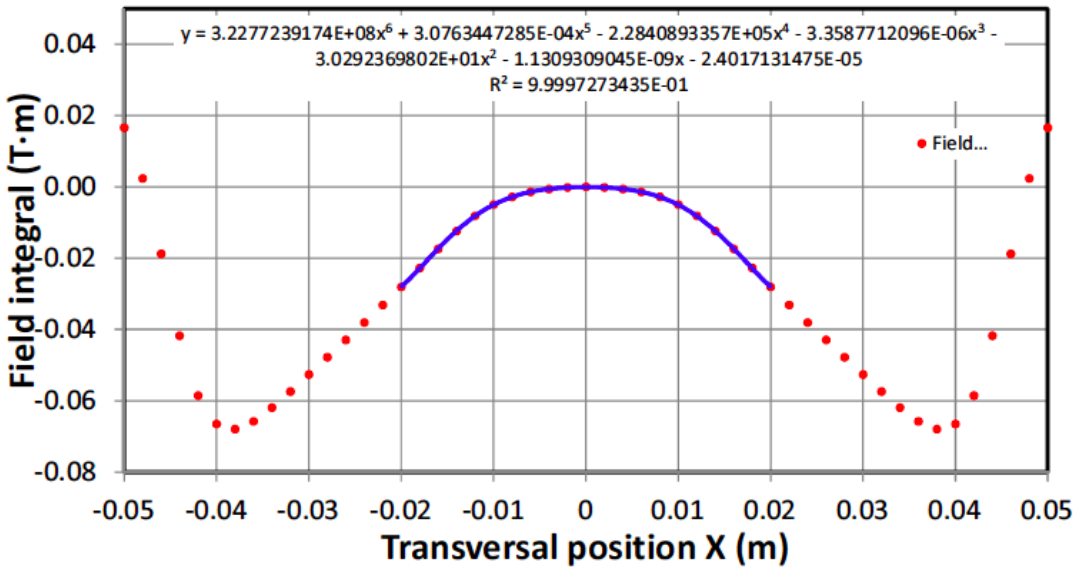

Figure 14: Field integral of the 3T wavelength shifter along the horizontal axis

The multipolar terms of the field integral expansion in the horizontal coordinate for the 3PW-1 wiggler are listed in Table 9.

Multipole	3PW-1
Dipole	$-2.40 \cdot 10^{-5}$ T·m
Quadrupole	-9.45·10 10 T
Sextupole	-30.329 T/m
Octupole	$-5.96 \cdot 10^{-7}$ T/m^2
Decapole	$-2.28 \cdot 10^{5}$ T/m^3
Dodecapole	$-6.84 \cdot 10^{-4}$ T/m^4
Tetradecapole	$3.23 \cdot 10^{8}$ T/m^5

Table 9: Multipolar terms of the 3-pole wavelength shifter

A study of the beam dynamics effects of this wiggler on the SESAME lattice [5] shows that the linear optics effect is negligible at 2.5 GeV and can easily be corrected at the injection energy (0.8 GeV) by varying the strength of nearby quadrupoles by less than 6%.

The effects of the sextupole and decapole terms however are quite strong already at 2.5 GeV and reduce the dynamic aperture in the horizontal plane below the value required for injection [4].

Multipolar components

SESAME is operated at a chromaticity corrected to +5 in both planes, in order to mitigate instabilities. The three-pole wavelength shifter's sextupole component is a factor of 3.43 larger than the SESAME standard focusing sextupole and a factor of 2.17 larger than the defocusing sextupole. It modifies the horizontal chromaticity from C_x = +5 to C_x = +1 and the vertical one from C_y = +5.0 to C_x = +5.22. The impact of the wiggler sextupole component is much larger in the horizontal plane than in the vertical one due to the large β_x and small β_y in the center of the short section.

After correcting both horizontal and vertical chromaticity to +5 by using the storage ring's sextupoles, the dynamic aperture was evaluated and is shown in Figure 15 (green line), compared with that of the ideal lattice (red line). The dynamic aperture is reduced, nevertheless it is still sufficiently larger than the physical aperture defined by the vacuum chamber (pink line).

When including also the decapole component, however, the dynamic aperture is strongly reduced (blue line in Figure 15) and, in the horizontal plane, becomes much smaller than the physical aperture.

Therefore, the decapole component of the three-pole wavelength shifter cannot be neglected and has to be reduced considerably.

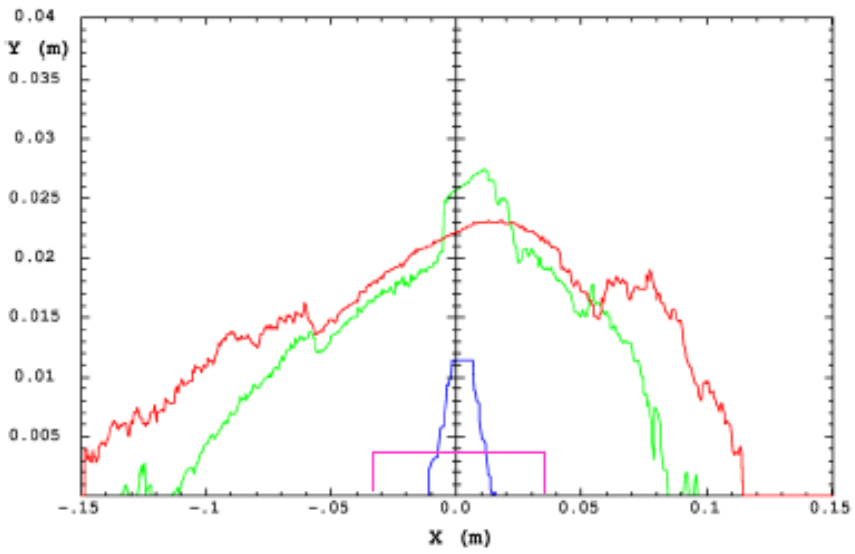

Figure 15: Dynamic aperture for the 3-pole wavelength shifter option. Red: Ideal lattice, green: effect of the ID without decapole effects, blue: ditto including decapole effects, pink: physical aperture

3 pole wavelength shifter design (3PW-2) with reduced multipolar terms

After the SESAME beam dynamics simulation, a further refined wiggler design with considerably reduced multipole terms (called 3PW-2), has been proposed by ALBA [5,6] see Figure16.

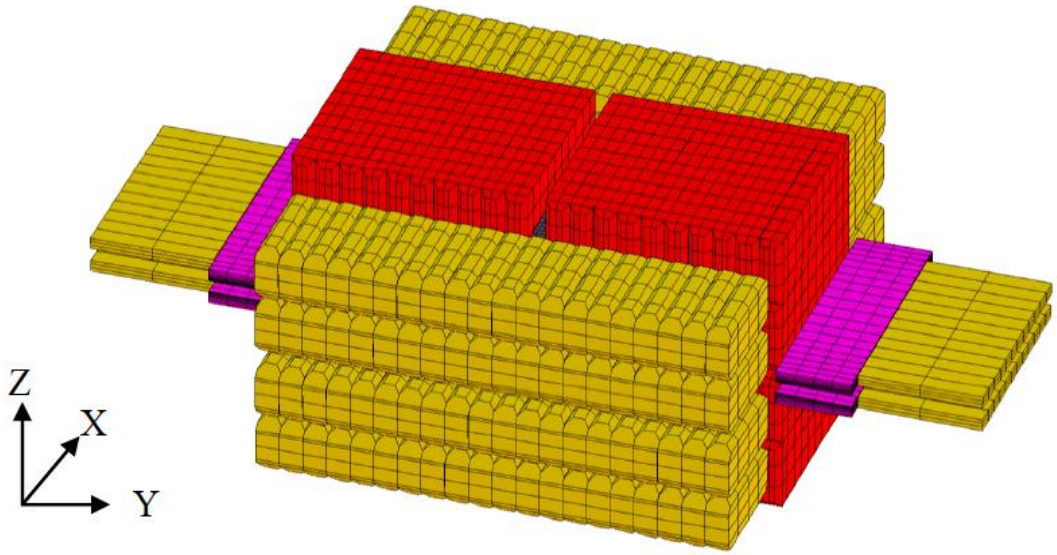

Figure: 16: Axis definition and magnetic model generated by RADIA. Red and yellow parts are NdFeB magnets. Pink parts are iron poles (there is another iron pole –grey– in the center). The overall length is 0.755 m, the overall width is 0. 400 m, the overall height is 0.331 m and the minimum gap is 11 mm.

The 3PW-2 design differs from 3PW-1 by its larger pole size to reduce the multipole field components and to mitigate the effects on the beam dynamics. Table 10 shows a comparison of the multipolar terms between the initial and the improved design

Multipole	3PW-1	3PW-2 (fit ± 60 mm)	3PW-2 (fit ± 20 mm)
Dipole	$-2.40 \cdot 10^{-5}$ T·m	$-5.78 \cdot 10^{-3}$ T·m	
Quadrupole	$-9.45 \cdot 10^{-}10$ T	$-3.58 \cdot 10^{-12}$ T	
Sextupole	-30.329 T/m	-1.76 T/m	-1.91 T/m
Octupole	$-5.96 \cdot 10^{-7}$ T/m^2	$5.27 \cdot 10^{-9}$ T/m^2	
Decapole	$-2.28 \cdot 10^{5}$ T/m^3	$-5.46 \cdot 10^{2}$ T/m^3	$-2.11 \cdot 10^{3}$ T/m^3
Dodecapole	$-6.84 \cdot 10^{-4}$ T/m^4	$-1.17 \cdot 10^{-6}$ T/m^4	
Tetradecapole	$3.23 \cdot 10^{8}$ T/m^5	-	3.29 x10^{5} T/m^5

Table 10: Multipolar terms of the 3-pole wavelength shifter design 3PW-1 and 3PW-2. The contribution of the multipole terms of 3PW-2 have been fitted for two different ranges of the horizontal aperture.

Figure 17 and 18 show the magnetic field of 3PW-1 on axis and its field integral on the transversal axis, respectively, the latter showing prominent modifications to improve the acceptance while reducing the multipolar components.

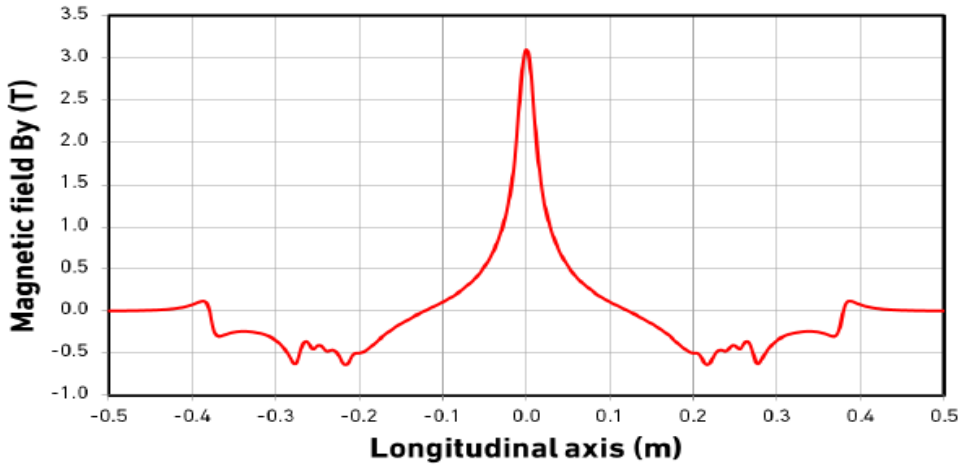

Figure 17: Magnetic field along the trajectory of the electron beam for 3PW-2.

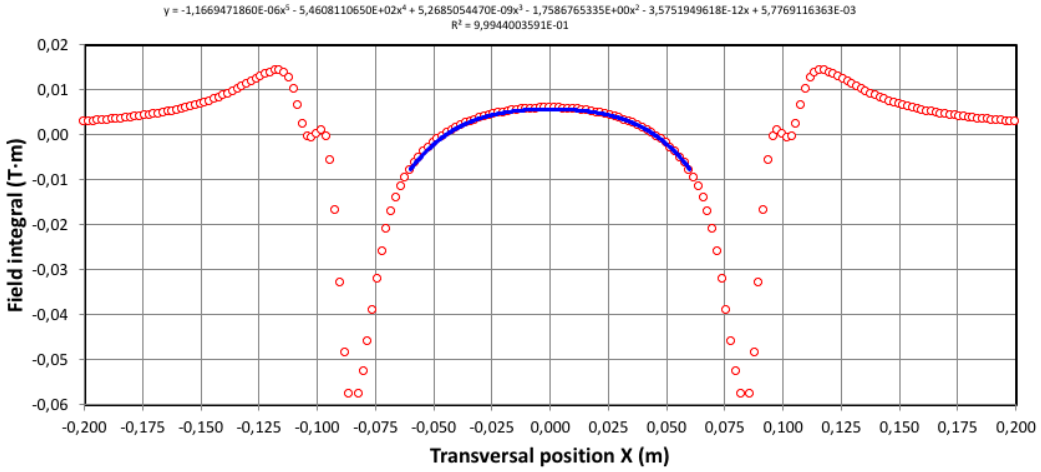

Fig. 18: 3PW-2 field integral along transversal axis

The emission spectrum, computed using the SPECTRA code and assuming an aperture of 1 mrad, is shown in Figure 19.

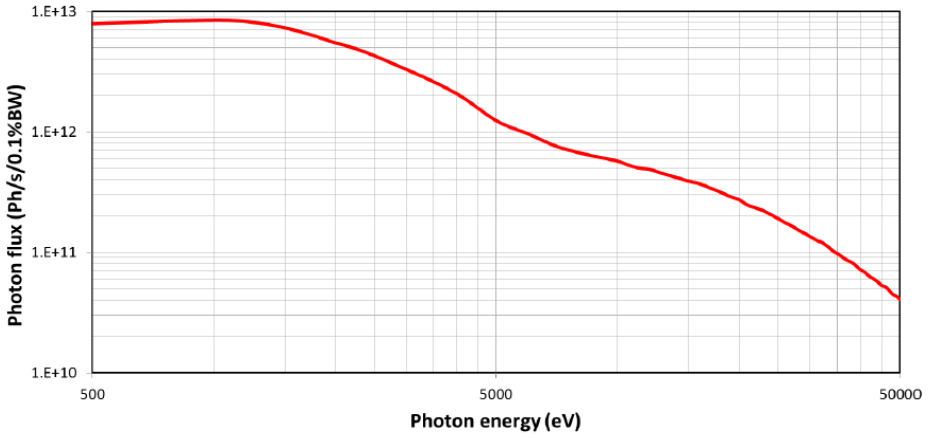

Figure 19: Photon beam spectrum emitted by the 3 pole wavelength shifter 3PW-2.

The multipolar terms of the field integral expansion in the horizontal coordinate for the 3PW-2 wiggler are listed in column 3 of Table 10, to be compared with the 3PW-1 wavelength shifter (column 2).

A preliminary study of the beam dynamics effects of the low multipole wiggler 3PW-2, using the sextupole and decapole terms listed in Table 10, shows that its effect within the injection aperture is negligible. On the other hand, if one carries out the multipole expansion in the region $\pm$ 20 mm, which is the actual ring aperture, one obtains larger values for the the sextupole, decapole and 14-pole terms, as shown in Table 10, column 4.

The dynamic aperture evaluated with the sextupole and decapole components (blue line), and including sextupole, decapole, and 14-pole components (green line), is shown in Fig. 20, compared with that of the ideal lattice (red line). The dynamic aperture is reduced, nevertheless it is still larger than the physical aperture defined by the vacuum chamber (pink line).

However, the new, multipolar terms reducing, model leads to a considerable increase of the attractive forces between the magnetic structures, passing from ~0.7 tons to ~2.3 tons.

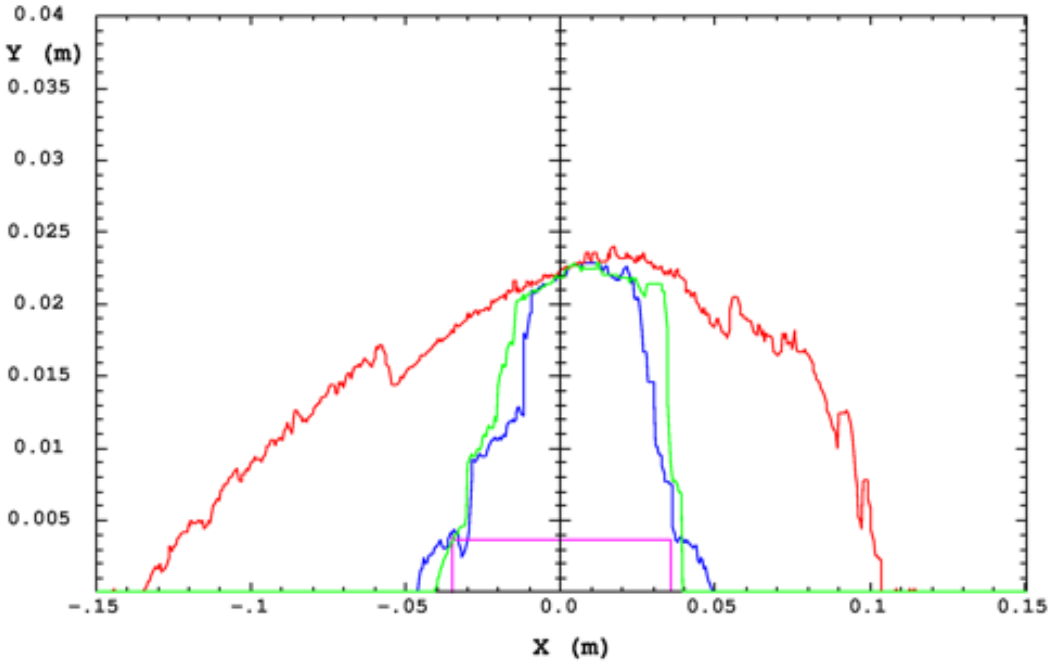

Fig. 20: Dynamic aperture for the 3 pole wavelength shifter 3PW/2. Unperturbed lattice (Red), dynamic aperture including sextupole, decapole components (blue), including as well 14-pole components (green).

SUMMARY AND CONCLUSIONS

A principal decision on the type of the BEATS x-ray source had already been taken at the BEATS kick-off meeting in March 2019.

The concept of a super-bend was rejected since it would have caused too much perturbation to the accelerator, in particular concerning the girder modification and the installation of two new quadrupoles and a new arc vacuum chamber.

The multipole (50 poles) wiggler was rejected since it would have most likely required a superconducting magnet with the heavy impact of the installation of a cryogenic system.

Therefore, it was decided to use as source a 3-pole wiggler with 3 T field to be installed in one of the short straight sections of the SESAME ring.

Two different wiggler models have been proposed so far (3PW-1 and 3PW-2), both out-vacuum, with 3 T peak field and a gap of 11 mm. The price of reducing the multipole components for such a device however is the increase of the attractive force, passing from ~0.7 tons to ~2.3 tons.

A very preliminary study of the beam dynamics effects of the low multipole wiggler 3PW-1 shows that the dynamic aperture is reduced when including the multipole terms generated by the wiggler but still it is larger than the ring physical aperture.

At present, we can state that a 3T field 3-pole wiggler is a suitable solution for the BEATS x-ray source and that the low multipole design 3PW-2 satisfies the requirements.

In the next 8 months work package 3 will address the following issues:

- Perform a complete study of the beam dynamics to evaluate the effect of the low-multipole 3-pole wavelength shifter on the SESAME lattice, including dynamic aperture and energy acceptance at operation (2.5 GeV) and at injection energy (0.8 GeV)
- Study the possibility of using a modified lattice like the ones proposed at the kick-off meeting (lower dispersion in all the short straight sections or in the wiggler straight section only and lower beta functions) in order to reduce the effects of the wiggler multipole terms on the beam.
- Evaluate the emitted photon spectrum taking into account all the details of the source.
- Explore the possibility of using the ESRF prototype of a 3 T wiggler (taking only one period), now disassembled, that could be refurbished [7]
- Evaluate the pros and cons of using a 2-pole wiggler instead of a 3-pole based design

REFERENCES

1) R. Bartolini, 'Update from WP3', BEATS kickoff meeting, Sesame 12 - 13 March 2019
2) J. Campmany, 'The Photon Source for the BEATS beamline at SESAME', BEATS kickoff meeting, Sesame 12 - 13 March 2019
3) https://sesame.org.jo/sites/default/files/images/sesame-publications/Technical_Notes/O-1.pdf
4) M. Attal, 'Tomography Beamline Photon Source in SESAME Storage Ring', 31/10/2018
5) J. Campmany, 'Technical specifications and conceptual design of a 3PW photon source for the BEATs beamline at SESAME syncrotron' *ALBA Project Document* AAD-IDBEATS-A-0002, 29 March 2019
6) M. Attal, 'Impact of the Proposed Wavelength Shifter on SESAME Beam Dynamics', May 31, 2019, updated on June 27, 2019
7) Nuclear Instruments and Methods in Physics Research A 421 (1999) 352–360